University of Nebraska - Lincoln
DigitalCommons@University of Nebraska - Lincoln

Alexei Gruverman Publications | Research Papers in Physics and Astronomy

12-2015

Contact resistance to $SrRuO_3$ and $La_{0.67}Sr_{0.33}MnO_3$ epitaxial films

Mohammad Abuwasib
University at Buffalo, mabuwasi@buffalo.edu

Hyungwoo Lee
University of Wisconsin-Madison

Alexei Gruverman
University of Nebraska-Lincoln, agruverman2@unl.edu

Chang-Beom Eom
University of Wisconsin-Madison, eom@engr.wisc.edu

Uttam Singisetti
University at Buffalo, uttamsin@buffalo.edu

Follow this and additional works at: http://digitalcommons.unl.edu/physicsgruverman

 Part of the Condensed Matter Physics Commons

Abuwasib, Mohammad; Lee, Hyungwoo; Gruverman, Alexei; Eom, Chang-Beom; and Singisetti, Uttam, "Contact resistance to $SrRuO_3$ and $La_{0.67}Sr_{0.33}MnO_3$ epitaxial films" (2015). *Alexei Gruverman Publications*. 60.
http://digitalcommons.unl.edu/physicsgruverman/60

This Article is brought to you for free and open access by the Research Papers in Physics and Astronomy at DigitalCommons@University of Nebraska - Lincoln. It has been accepted for inclusion in Alexei Gruverman Publications by an authorized administrator of DigitalCommons@University of Nebraska - Lincoln.

Contact resistance to $SrRuO_3$ and $La_{0.67}Sr_{0.33}MnO_3$ epitaxial films

Mohammad Abuwasib,[1] Hyungwoo Lee,[2] Alexei Gruverman,[3] Chang-Beom Eom,[2] and Uttam Singisetti[1]
[1]*Department of Electrical Engineering, University at Buffalo, Buffalo, New York 14260, USA*
[2]*Department of Materials Science and Engineering, University of Wisconsin-Madison, Madison, Wisconsin 53706, USA*
[3]*Departments of Physics and Astronomy, University of Nebraska–Lincoln, Nebraska 68588, USA*

(Received 25 September 2015; accepted 7 December 2015; published online 17 December 2015)

Contact resistance to the metallic oxide electrodes, $SrRuO_3$ (SRO) and $La_{0.67}Sr_{0.33}MnO_3$ (LSMO), is an important parameter that affects the ferroelectric tunnel junction (FTJ) device performance. We have systematically studied the contact resistance between metallic oxide electrodes (SRO, LSMO) and contact metal overlayers (Ti, Pt) after exposure to various processing environments. Specific contact resistivity (ρ_c) for Ti and Pt contact metals and the sheet resistance (R_{sh}) of the metallic oxides are measured after exposure to different reactive ion plasma process steps. Sheet resistance degradation was observed for both SRO and LSMO films after exposure to plasma treatment. Severe contact resistance degradation was observed for Ti contacts as compared to Pt after reactive ion etching on LSMO films. The effect of oxygen (O_2) plasma on LSMO was observed to be most severe with non-ohmic behavior with Ti contacts, which can affect the functionality of FTJ devices. Finally, the thermal stability of contacts was investigated, Pt contacts to SRO show low resistance ohmic behavior even after annealing at 900 °C, making it a suitable contact for FTJ devices. © *2015 AIP Publishing LLC*. [http://dx.doi.org/10.1063/1.4938143]

Ferroelectric Tunnel Junction (FTJ) devices are promising candidates for beyond CMOS applications that can be used for both non-volatile memory and non-volatile logic.[1–4] The tunneling electroresistance (TER) effect in an FTJ leads to large off-on ratios.[5–8] The FTJ device has several advantages over traditional ferroelectric random access memory (FeRAM) including large off-on resistance ratio, non-destructive readout, ultra-low power operation, high storage density, and nanometer size scaling.[1–4,7,9–11] The structure of FTJ is essentially a metal-insulator-metal (M_1-FE-M_2) tunnel junction with a ferroelectric (FE) insulator as the tunnel barrier. Several groups have reported functional FTJ devices with $BaTiO_3$ (BTO) and $BiFeO_3$ (BFO) as the ferroelectric barrier.[6,7,10–13] BTO is widely used as the FE barrier because it has low critical thickness which can lead to low power FTJ devices. Moreover, the critical thickness of BTO can be further reduced by applying a biaxial strain on it.[7,14] In addition to the ferroelectric barrier, the choice of the top and bottom metals is also important for large off-on resistance ratio and low power operation.[11,15,16] The workfunction difference between the metals and the screening lengths in the metals can enhance the TER.[5] The top metal is often Co/Au or Pt deposited by electron beam evaporation.[6,10–12] While the bottom metal is usually metallic oxides such as $SrRuO_3$ (SRO)[17] or $La_{0.67}Sr_{0.33}MnO_3$ (LSMO) with lattice matching to the FE barrier which enables epitaxial growth of defect free BTO.[18]

Lattice matching of the BTO ferroelectric barrier is essential for the bottom metal. SRO, the single crystal isotropic metallic oxide is preferable as the bottom electrode metal in the FTJ heterostructure as it is chemically and thermally stable compared to cuprite superconductor based electrodes.[18,19] Moreover, undoped SRO is one of the very few complex metallic oxides that provides smooth surface for epitaxial growth of single crystal BTO film which may improve ferroelectric fatigue.[20] Strain engineering for critical thickness of BTO reported by Choi *et al.*[14] opens up the possibility of using other complex oxide metal as bottom electrode beside SRO. Garcia *et al.* showed large TER in a strained BTO using LSMO layer as bottom electrode which shows great promise for high density FTJ integration.[7] Due to the above-mentioned reasons, a majority of reported FTJ devices use either SRO or LSMO as bottom electrode. The reported FTJ devices were measured using the conductive atomic force microscope (AFM) tip as an electrode.[6,7,10–12,21] However, in order to analyze the scalability, CMOS compatibility, high speed operation, and reliability of FTJ devices full scale integration are required. A CMOS compatible FTJ integration process is recently reported with BTO as ferroelectric material and LSMO as bottom electrode.[22] It was shown the contact resistance to LSMO increased significantly after fabrication severely affecting the device performance. As integration of FTJs with CMOS is important for building non-volatile memory and logic circuits, the technological and processing challenges need to be addressed. Robust and stable contacts to FTJ is necessary; however, there is no report of contact resistance to metallic oxide electrodes. Integrated devices with BFO ferroelectric barrier has also been reported recently, however contact resistance issues were not addressed.[13] In this letter, we report the systematic investigation of ohmic contacts to SRO and LSMO metallic oxide epitaxial films for FTJ integration. This study will also benefit other emerging devices based on complex oxides including ferroelectric devices,[23] magnetic tunnel junction devices,[24] and spintronic devices[25] that use metallic oxides SRO and LSMO.

We study the contact metals Ti and Pt on SRO and LSMO. Ti is widely used as an adhesive and contact layer in semiconductor fabrication, while Pt is selected due to its

 © 2015 AIP Publishing LLC

resistance to oxidation. We use circular transmission line method (CTLM) to extract the contact parameters: specific contact resistivity ρ_c, transfer length L_T, and the sheet resistance R_{sh}. For CTLM studies, 50 nm thick single crystalline SRO and LSMO thin films were grown epitaxially on (001) STO and (110) NGO substrates, respectively, by pulsed laser deposition (PLD).[12,14] Reflection high-energy electron diffraction (RHEED) has been used for in-situ monitoring of the layer-by-layer growth process. Before deposition, the STO substrates were etched using buffered HF acid for 60 s to obtain Ti-termination, and then were annealed in oxygen at 1000 °C for 6 h to create atomically smooth surfaces with single-unit-cell-height steps. The NGO substrates were annealed at 1100 °C for 4 h without BHF etching. CTLM structures were defined on SRO and LSMO samples using electron beam lithography and lift-off with Pt and Ti. In the CTLM structure, the radius (r) of the circular inner contact was kept constant ($r = 75\ \mu$m). The contact separation (s) was varied from 2.5 μm to 25 μm. A scanning electron microscopy (SEM) image of patterned CTLM is shown in Fig. 1(a) for a contact separation of 10 μm.

In order to check the stability of the contacts with respect to fabrication steps, blanket SRO/LSMO films (~50 nm) were exposed to various etch chemistries in an inductively coupled plasma (ICP) reactive ion etching (RIE) system. Chlorine (Cl_2) based RIE together with argon (Ar) for physical milling is a very effective etch for perovskite oxide such as LSMO.[26] To study the effect of chlorine chemistry, we used BCl_3 and Ar gas mixture with flow rates 15 and 10 sccm, respectively. ICP power was set 100 W to create dense plasma whereas RIE power was chosen 200 W with chamber pressure 20×10^{-3} Torr to ensure anisotropic etching with vertical sidewall profile. This etch process has been used in fabrication of integrated FTJs.[22] The etching time was chosen 45 s to minimize the damage on the SRO/LSMO surfaces. A thin layer (~6 nm) of SRO/LSMO film was etched due to this with a measured etch rate of ~8 nm/min. The AFM images of SRO and LSMO surface after applying BCl_3/Ar based RIE plasma is shown in Fig. 2, no significant roughening is observed for both SRO and LSMO films. Oxygen (O_2) plasma is used to remove polymers formed during photo-lithography process. In order to evaluate the effect of O_2 plasma, we applied 20 sccm O_2 flow for

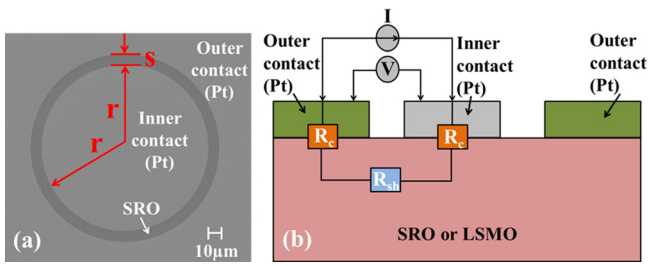

FIG. 1. (a) An SEM micrograph of a CTLM structure patterned on a 50 nm SRO film using a Pt contact metal of thickness 25 nm. Circular inner contact (Pt) radius, $r = 75\ \mu$m with the separation, $s = 10\ \mu$m from the outer contact (Pt). (b) Cross-section schematic of four-point probe configuration used to measure resistance (R_T) in CTLM structure. A current was applied between the outer probes using current source (I) whereas voltage was measured between the inner probes using voltmeter (V).

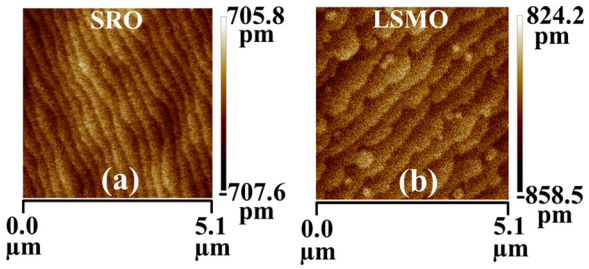

FIG. 2. AFM images of (a) SRO and (b) LSMO after applying BCl_3/Ar plasma treatment.

45 s instead of BCl_3/Ar on blanket SRO/LSMO films prior to forming Pt and Ti contacts on it.

The current-voltage (I-V) measurement on the CTLM structure was carried out using Agilent 4155B parameter analyzer, and a four-point probe technique was used for extracting contact resistance from CTLMs.[27] As seen in Fig. 1(b), a current was applied between the outer probes using current source (I), whereas voltage was measured between the inner probes using voltmeter (V). This technique removes the contribution of the probe resistance from the measurement. Both Ti and Pt contacts to untreated SRO and LSMO films show ohmic behavior with no hysteresis or resistive switching. The total four-point probe resistance (R_T) as a function of contact separation (s) for Pt contact on SRO and LSMO before and after applying RIE is shown in Fig. 3 from which the sheet resistance (R_{sh}) and specific contact resistivity (ρ_c) is extracted.[27] Table I lists the extracted contact resistance parameters for SRO and LSMO for different contacts (Pt/Ti) and process conditions.

Table I shows that the sheet resistance (R_{sh}) of SRO and LSMO films is increased after exposure to BCl_3/Ar RIE and O_2 plasma. The etch depth during the BCl_3/Ar RIE was verified to be 6 nm on control samples by AFM measurements. With the initial thickness of 50 nm, this would lead to 12% increase in the R_{sh} for both SRO and LSMO due to the reduction in film thickness. However, after BCl_3/Ar plasma treatment, the R_{sh} increased more than 12% for both LSMO and SRO films. For Pt contact to SRO the sheet resistance (R_{sh}) increased by ~120 Ω/sq., whereas for LSMO it increased by ~525 Ω/sq. from untreated films, although the reduction in thickness is small. Similarly, large increase in R_{sh} was observed for LSMO (~1.6 KΩ/sq.) and SRO (0.16 KΩ/sq.) films after applying O_2 plasma although there is no effective etching of the films.

The large increase of R_{sh} can be attributed to the surface damage caused by the ions during the plasma processing.

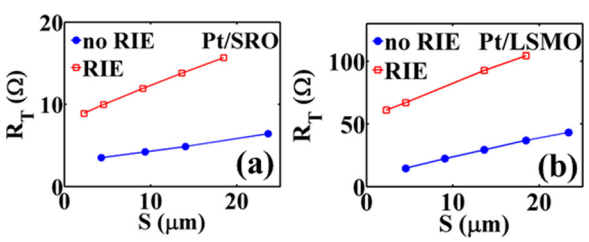

FIG. 3. CTLM four-point probe measurement of total resistance (R_T) vs. contact separation (s) for (a) Pt/SRO (b) Pt/LSMO contacts without RIE (blue) and with RIE (red).

TABLE I. Extracted specific contact resistivity (ρ_c), sheet resistance (R_{sh}), and transfer length (L_T) of Pt and Ti contacts to SRO and LSMO under different processing conditions.

Contact	No RIE	BCl_3/Ar RIE	O_2 plasma
Pt/SRO	$\rho_c = 6 \times 10^{-5}$ ($\Omega\,cm^2$) $R_{sh} = 70\,\Omega$/sq. $L_T = 9.4\,\mu m$	$\rho_c = 1.7 \times 10^{-4}$ ($\Omega\,cm^2$) $R_{sh} = 190\,\Omega$/sq. $L_T = 9.6\,\mu m$	$\rho_c = 1.2 \times 10^{-4}$ ($\Omega\,cm^2$) $R_{sh} = 235\,\Omega$/sq. $L_T = 7.3\,\mu m$
Pt/LSMO	$\rho_c = 5 \times 10^{-5}$ ($\Omega\,cm^2$) $R_{sh} = 675\,\Omega$/sq. $L_T = 2.7\,\mu m$	$\rho_c = 1.2 \times 10^{-3}$ ($\Omega\,cm^2$) $R_{sh} = 1.2\,K\Omega$/sq. $L_T = 10\,\mu m$	$\rho_c = 4.4 \times 10^{-2}$ ($\Omega\,cm^2$) $R_{sh} = 2.3\,K\Omega$/sq. $L_T = 45\,\mu m$
Ti/SRO	$\rho_c = 1.7 \times 10^{-4}$ ($\Omega\,cm^2$) $R_{sh} = 100\,\Omega$/sq. $L_T = 13.2\,\mu m$	$\rho_c = 1.3 \times 10^{-4}$ ($\Omega\,cm^2$) $R_{sh} = 270\,\Omega$/sq. $L_T = 7\,\mu m$	NA
Ti/LSMO	$\rho_c = 3 \times 10^{-3}$ (Ω-cm^2) $R_{sh} = 850\,\Omega$/sq. $L_T = 20\,\mu m$	Non-ohmic I-V	Non-ohmic I-V

Increase in R_{sh} due to the ion damage has been reported in a number of III–V semiconductors.[28–31] The surface damage creates surface states[31] which can deplete the carriers in the film increasing R_{sh}. Similar damage on the SRO and LSMO surfaces can lead to high sheet resistance. In addition to surface damage, in the case of perovskite oxide films (SRO/LSMO), oxygen and metal vacancy can be created during the plasma process which will again increase the sheet resistance. Increase of R_{sh} in an LSMO film has been reported by thermal annealing and Si implantation, which has been attributed to oxygen loss and conversion of Mn^{4+} ions to Mn^{3+} ions.[32,33] Similarly for SRO films, Ru and oxygen vacancy will lead to loss of carrier and increase in the sheet resistance.[17,34,35]

The specific contact resistivities (ρ_c) of Pt contact for untreated SRO and LSMO are $6 \times 10^{-5}\,\Omega\,cm^2$ and $5 \times 10^{-5}\,\Omega\,cm^2$, respectively, which after exposure to BCl_3/Ar plasma increased by 3 times and 25 times, respectively. On the other hand, Ti/LSMO contacts become non-ohmic (Fig. 4(a)). Severe contact degradation was observed for Ti contacts to LSMO after O_2 plasma exposure, Ti/ LSMO contacts become Schottky type with non-linear I-V characteristics (Fig. 4(b)) which will severely impact an FTJ device operation with LSMO electrodes.[22] In contrast, Pt contacts to LSMO remain ohmic with increased ρ_c of $4.4 \times 10^{-2}\,\Omega\,cm^2$. The degradation of ρ_c of Pt and Ti contacts to SRO and LSMO can be attributed to the surface damage, surface segregation, and interface reaction properties after RIE. The contact resistance is determined by the barrier height and depletion width formed between metals (Pt/Ti) and metallic oxides (SRO/LSMO) surface.[27] As discussed previously, the R_{sh} is increased after RIE for SRO and LSMO films, which indicate a larger depletion width, hence an increased ρ_c. After plasma treatment the LSMO surface may change into SrO, SrO_3, MnO, MnO_2.[36–38] When Ti is deposited onto the segregated LSMO surface, oxygen in MnO or MnO_2 reacts with Ti forming a TiO_2 Schottky barrier[39] which would make I-V non-ohmic as observed in Fig. 4. However, no such reaction is possible for Pt contacts to etched LSMO, which remain ohmic with an increased $\rho_c \sim 1.2 \times 10^{-3}$ ($\Omega\,cm^2$).

Finally, the thermal stability of Ti and Pt contacts to SRO/LSMO films was analyzed by annealing the contacts in a rapid thermal anneal (RTA) system for 90 s at elevated temperatures under a N_2 atmosphere. Figure 5 shows the I-V curves of Ti contacts to SRO and LSMO after annealing at elevated temperatures. Although Ti forms an ohmic contact on untreated LSMO at room temperature, it shows high resistance Schottky type I-V with suppressed current ($<100\,\mu A$) after anneal at 300 °C (Fig. 5(b)). The rapid degradation of Ti/LSMO contacts with annealing at elevated temperatures is due to acceleration of surface segregation[38,40] and the enhanced diffusion of O_2 into Ti forming TiO_2 Schottky barrier.[39] However, Ti/SRO contacts remain low resistance ($\sim 1\,K\Omega$) after annealing at 500 °C due to its high thermodynamic stability.[41] Beyond which the contacts become highly resistive (Fig. 5(a)) with nonlinearity due to the decomposition of SRO[42,43] and the subsequent reaction of O_2 with Ti and formation of TiO_2 Schottky barrier. In contrast, Pt contacts remain ohmic for

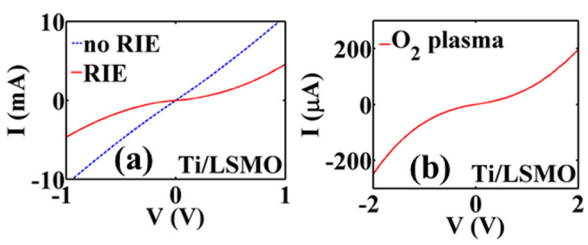

FIG. 4. Two-probe current voltage (I-V) characteristics of Ti/LSMO contact after applying 45 s (a) BCl_3, Ar based plasma and (b) O_2 plasma.

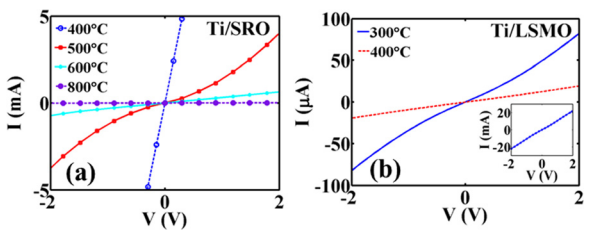

FIG. 5. Two-probe I-V characteristics of untreated (a) Ti/SRO (b) Ti/LSMO contacts after rapid thermal annealing (RTA) process. The RTA was applied for 90 s in N_2 ambient. The separation between inner contact and outer contact, s = 15 μm. Inset: I-V characteristics of untreated Ti/LSMO contact at room temperature.

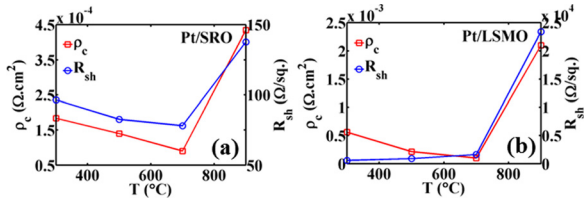

FIG. 6. Specific contact resistivity (ρ_c) and sheet resistance (R_{sh}) of Pt contact with (a) SRO and (b) LSMO after rapid thermal annealing (RTA) process.

both SRO and LSMO even after annealing at 900 °C due to its low reactivity with oxygen. Figure 6 shows the extracted specific contact resistivity (ρ_c) and sheet resistance (R_{sh}) of Pt/SRO and Pt/LSMO contacts with annealing temperatures (T). Specific contact resistivity (ρ_c) first decreases with increased annealing temperatures by stabilizing the contacts and reaches a minimum value at $9 \times 10^{-5}\,\Omega\,cm^2$ and $1 \times 10^{-4}\,\Omega\,cm^2$ for Pt/SRO and Pt/LSMO contacts, respectively. However, R_{sh} of LSMO severely degrades to 1.6 KΩ/sq. at 700 °C due to high temperature metal to insulator phase transition of LSMO films,[33] whereas R_{sh} remains low for SRO (75Ω/sq.) verifying its thermal stability. Decrease of ρ_c for a Pt/SRO contact by thermal annealing can be useful for getting optimum performance of integrated FTJ devices with SRO electrodes, whereas increase of R_{sh} of LSMO films at high temperature could be detrimental for integrated FTJ with LSMO electrodes during high temperature processing.

In conclusion, we investigated the contact resistance characteristics of SRO and LSMO with different contact metals (Pt/Ti) which is important for FTJ integration. We measure the stability of these contacts for different plasma treatments used during fabrication steps and annealing at elevated temperatures. From these measurements, it is clear that SRO forms ohmic contacts to Ti and Pt even after exposure to various plasma chemistries with minimal degradation in the contact resistance whereas LSMO contacts show degradation in the presence of plasma treatment and annealing at elevated temperatures which makes it technologically challenging for future FTJ integration.

This project was supported by the Semiconductor Research Corporation (SRC) through the Center for Nanoferroic Devices (CNFD), an SRC-NRI Nanoelectronics Research Initiative Center under Task ID 2398.002. A portion of this work was performed in the University at Buffalo Electrical Engineering Cleanroom and the Materials Characterization Laboratory, part of the university's Shared Instrumentation Laboratories.

[1]E. Y. Tsymbal and A. Gruverman, Nat. Mater. **12**(7), 602–604 (2013).
[2]A. M. Ionescu, Nat. Nanotechnol. **7**(2), 83–85 (2012).
[3]A. Chen, J. Hutchby, V. Zhirnov, and G. Bourianoff, *Emerging Nanoelectronic Devices* (John Wiley & Sons, 2014).
[4]J. A. Hutchby, R. Cavin, V. Zhirnov, J. E. Brewer, and G. Bourianoff, Computer **41**(5), 28–32 (2008).
[5]M. Y. Zhuravlev, R. F. Sabirianov, S. Jaswal, and E. Y. Tsymbal, Phys. Rev. Lett. **94**(24), 246802 (2005).
[6]A. Gruverman, D. Wu, H. Lu, Y. Wang, H. W. Jang, C. M. Folkman, M. Y. Zhuravlev, D. Felker, M. Rzchowski, C. B. Eom, and E. Y. Tsymbal, Nano Lett. **9**(10), 3539–3543 (2009).
[7]V. Garcia, S. Fusil, K. Bouzehouane, S. Enouz-Vedrenne, N. D. Mathur, A. Barthelemy, and M. Bibes, Nature **460**(7251), 81–84 (2009).
[8]P. Maksymovych, S. Jesse, P. Yu, R. Ramesh, A. P. Baddorf, and S. V. Kalinin, Science **324**(5933), 1421–1425 (2009).
[9]A. Chanthbouala, V. Garcia, R. O. Cherifi, K. Bouzehouane, S. Fusil, X. Moya, S. Xavier, H. Yamada, C. Deranlot, N. D. Mathur, M. Bibes, A. Barthélémy, and J. Grollier, Nat. Mater. **11**(10), 860–864 (2012).
[10]A. Chanthbouala, A. Crassous, V. Garcia, K. Bouzehouane, S. Fusil, X. Moya, J. Allibe, B. Dlubak, J. Grollier, S. Xavier, C. Deranlot, A. Moshar, R. Proksch, N. D. Mathur, M. Bibes, and A. Barthelemy, Nat. Nanotechnol. **7**(2), 101–104 (2012).
[11]Z. Wen, C. Li, D. Wu, A. Li, and N. Ming, Nat. Mater. **12**(7), 617–621 (2013).
[12]D. J. Kim, H. Lu, S. Ryu, C. W. Bark, C. B. Eom, E. Y. Tsymbal, and A. Gruverman, Nano Lett. **12**(11), 5697–5702 (2012).
[13]S. Boyn, S. Girod, V. Garcia, S. Fusil, S. Xavier, C. Deranlot, H. Yamada, C. Carrétéro, E. Jacquet, M. Bibes, A. Barthélémy, and J. Grollier, Appl. Phys. Lett. **104**(5), 052909 (2014).
[14]K. J. Choi, M. Biegalski, Y. L. Li, A. Sharan, J. Schubert, R. Uecker, P. Reiche, Y. B. Chen, X. Q. Pan, V. Gopalan, L.-Q. Chen, D. G. Schlom, and C. B. Eom, Science **306**(5698), 1005–1009 (2004).
[15]R. Soni, A. Petraru, P. Meuffels, O. Vavra, M. Ziegler, S. K. Kim, D. S. Jeong, N. A. Pertsev, and H. Kohlstedt, Nat. Commun. **5**, 5414 (2014).
[16]X. S. Gao, J. M. Liu, K. Au, and J. Y. Dai, Appl. Phys. Lett. **101**(14), 142905 (2012).
[17]G. Koster, L. Klein, W. Siemons, G. Rijnders, J. S. Dodge, C.-B. Eom, D. H. Blank, and M. R. Beasley, Rev. Mod. Phys. **84**(1), 253 (2012).
[18]R. Ramesh, A. Inam, W. Chan, B. Wilkens, K. Myers, K. Remschnig, D. Hart, and J. Tarascon, Science **252**(5008), 944–946 (1991).
[19]C. Eom, R. Cava, R. Fleming, J. M. Phillips, J. Marshall, J. Hsu, J. Krajewski, and W. Peck, Science **258**(5089), 1766–1769 (1992).
[20]C. Eom, R. Van Dover, J. M. Phillips, D. Werder, J. Marshall, C. Chen, R. Cava, R. Fleming, and D. Fork, Appl. Phys. Lett. **63**(18), 2570–2572 (1993).
[21]Z. Wen, L. You, J. Wang, A. Li, and D. Wu, Appl. Phys. Lett. **103**(13), 132913 (2013).
[22]M. Abuwasib, H. Lee, P. Sharma, C.-B. Eom, A. Gruverman, and U. Singisetti, in *2015 73rd Annual Device Research Conference (DRC)* (IEEE, 2015), pp. 45–46.
[23]M. W. J. Prins, K. O. Grosse-Holz, G. Müller, J. F. M. Cillessen, J. B. Giesbers, R. P. Weening, and R. M. Wolf, Appl. Phys. Lett. **68**(25), 3650–3652 (1996).
[24]G. Herranz, B. Martínez, J. Fontcuberta, F. Sánchez, M. V. García-Cuenca, C. Ferrater, and M. Varela, J. Appl. Phys. **93**(10), 8035–8037 (2003).
[25]M. Bowen, M. Bibes, A. Barthélémy, J.-P. Contour, A. Anane, Y. Lemaître, and A. Fert, Appl. Phys. Lett. **82**(2), 233–235 (2003).
[26]K. Lee, K. Jung, H. Cho, D. Kumar, S. Pietambaram, R. Singh, P. Hogan, K. Dahmen, Y. Hahn, and S. Pearton, J. Electrochem. Soc. **146**(7), 2748–2751 (1999).
[27]D. K. Schroder, *Semiconductor Material and Device Characterization* (John Wiley & Sons, 2006).
[28]S. J. Pearton, J. W. Lee, J. D. MacKenzie, C. R. Abernathy, and R. J. Shul, Appl. Phys. Lett. **67**(16), 2329–2331 (1995).
[29]F. Ren, J. W. Lee, C. R. Abernathy, S. J. Pearton, C. Constantine, C. Barratt, and R. J. Shul, Appl. Phys. Lett. **70**(18), 2410–2412 (1997).
[30]F. Ren, J. Lee, C. Abernathy, S. Pearton, C. Constantine, C. Barratt, and R. Shul, J. Vac. Sci. Technol. B **15**(4), 983–989 (1997).
[31]R. J. Shul, M. L. Lovejoy, A. G. Baca, J. C. Zolper, D. J. Rieger, M. J. Hafich, R. F. Corless, and C. B. Vartuli, J. Vac. Sci. Technol. A **13**(3), 912–917 (1995).
[32]M. L. Wilson, J. M. Byers, P. C. Dorsey, J. S. Horwitz, D. B. Chrisey, and M. S. Osofsky, J. Appl. Phys. **81**(8), 4971–4973 (1997).
[33]A. Urushibara, Y. Moritomo, T. Arima, A. Asamitsu, G. Kido, and Y. Tokura, Phys. Rev. B **51**(20), 14103 (1995).
[34]H. Masahiko, O. Choichiro, I. Kazushige, and T. Kazumasa, Jpn. J. Appl. Phys., Part 1 **35**(12R), 6212 (1996).
[35]W. Siemons, G. Koster, A. Vailionis, H. Yamamoto, D. H. A. Blank, and M. R. Beasley, Phys. Rev. B **76**(7), 075126 (2007).
[36]R. Bertacco, J. P. Contour, A. Barthélemy, and J. Olivier, Surf. Sci. **511**(1–3), 366–372 (2002).
[37]M. P. de Jong, I. Bergenti, V. Dediu, M. Fahlman, M. Marsi, and C. Taliani, Phys. Rev. B **71**(1), 014434 (2005).

[38]T. T. Fister, D. D. Fong, J. A. Eastman, P. M. Baldo, M. J. Highland, P. H. Fuoss, K. R. Balasubramaniam, J. C. Meador, and P. A. Salvador, Appl. Phys. Lett. **93**(15), 151904 (2008).
[39]N. Homonnay, K. J. O'Shea, C. Eisenschmidt, M. Wahler, D. A. MacLaren, and G. Schmidt, ACS Appl. Mater. Interfaces **7**(40), 22196–22202 (2015).
[40]H. Jalili, Y. Chen, and B. Yildiz, ECS Trans. **28**(11), 235–240 (2010).
[41]T. Shimizu and T. Kawakubo, Jpn. J. Appl. Phys., Part 2 **40**(2A), L117 (2001).
[42]D. Halley, C. Rossel, D. Widmer, H. Wolf, and S. Gariglio, Mater. Sci. Eng., B **109**(1–3), 113–116 (2004).
[43]J. Shin, S. V. Kalinin, H. N. Lee, H. M. Christen, R. G. Moore, E. W. Plummer, and A. P. Baddorf, Surf. Sci. **581**(2–3), 118–132 (2005).